Lifetime Prediction of IGBT Modules in Suspension Choppers of Medium/Low-Speed Maglev Train Using an Energy-Based Approach

Xin Yang, *Member, IEEE*, Zhikai Lin, Jingfang Ding, and Zhiqiang Long

***Abstract*—Maglev trains attracted to suspend above tracks without mechanical contact is a promising type of track transportation. Suspension choppers with levitation magnets resembling wheels of traditional trains or tires of automobiles are responsible for levitation and support of maglev trains. With successful launch of the first Chinese medium/low-speed maglev line, lifetime prediction of power devices in suspension choppers becomes a crucial topic. This paper analyzes the lifetimes under two typical daily mission profiles of suspension choppers. Using look-up tables of IGBT/diode losses, a widely used *RC* thermal network is established. A test rig is built to measure the IGBT/diode transient case temperature and extract the thermal impedance of a heat sink. Therefore, the junction temperatures under these typical mission profiles are estimated. Using comprehensive equations to describe solder behavior, the stress–strain curves under different temperature profiles can be plotted by means of Clech's algorithm. Finally, an energy-based approach is utilized for lifetime evaluation. The daily mission profile where maglev trains operate without landing during operation hours is expected to survive much longer.**

***Index Terms*—IGBT, lifetime prediction, maglev trains, reliability, suspension choppers.**

I. Introduction

MAGLEV trains are an environmentally friendly type of track transportation with great advantages including low traction energy consumption (no mechanical friction), low noise, ride comfort, and so on. While high-speed maglev trains have integrated levitation and propulsion systems requiring more sophisticated control systems, medium/low-speed maglev trains composed of separated levitation and propulsion systems as shown in Fig. 1(a) are much simpler [1], [2]. The general suspension control principle is shown in Fig. 1(b). The difference between the actual gap fed back by gap sensors and a reference air gap is sent into a control DSP where the required duty cycle is calculated. The acceleration sensor is used to provide an extra feedback loop for stability consideration. Then, it is suspension choppers that generate levitation currents that flow into the electromagnets producing a desired magnetic force to levitate the train stably. Utilizing linear induction motors for propulsion, the maglev train could run up to a maximum speed of 110 km/h. This medium/low-speed maglev technique has a broad application prospect with advantages of lower construction cost, lower maintenance expenses, smaller turning radius, and better climbing ability compared with the conventional railway transportation at comparable speeds [1]–[3]. Recently, efforts are made to increase its operation speed up to 200 km/h [4].

Changsha Maglev Express (CME), the first domestic medium/low-speed maglev commercial line in China/the longest maglev line of the world, started operation in 2016. It stretches over 18.55 km and runs among Changsha International Airport, Langli, and Changsha South Railway Station. The reliability of a tire-resembling suspension control system is of crucial importance as it is directly related to safe operation. For high-speed maglev trains, reliability of suspension control systems is normally considered by using redundant hardware (control DSPs and sensors), and medium/low-speed maglev trains developed in CME follow a similar approach. However, there is rare investigation on the reliability of suspension choppers for high-speed or medium/low-speed applications. No redundant suspension chopper is used so far [1]–[4]. As the medium/low-speed maglev train was just put into commercial applications, lifetime prediction of suspension choppers requires full investigation. Prognostics of key power modules within suspension choppers, like other mission-critical systems such as avionics, high-speed rail, and offshore wind turbines, become significant [5]. In such a practical system, no failure is acceptable until the next maintenance period. Scientific guidance for health condition monitoring, maintenance, and repair is demanded.

Traditionally, lifetime estimation of power modules has relied on historical field data in handbooks and accelerated lifetime testing data. There are various handbooks based on constant failure rate models, for example, the Military-Handbook-217F [6]. Those models are simple but inappropriate, since they are based on an assumption of constant failure rates and more importantly, the impact of temperature excursions cannot be considered [6]. Empirical lifetime models are normally developed from accelerated lifetime data [7]–[12] or deduced from experience and large

Manuscript received July 14, 2017; revised December 3, 2017 and January 8, 2018; accepted February 23, 2018. Date of publication March 6, 2018; date of current version November 19, 2018. This work was supported in part by the National Natural Science Foundation of China under Grant 51607182, in part by the 13th Five-Year National Key R&D Program of China under Grant 2016YFB1200601-B11, and in part by the Maglev Technology Research Center of Hunan Province, China (Project: research on self-diagnostics and maintenance for middle-speed maglev controller). Recommended for publication by Associate Editor H. Wang. *(Corresponding author: Xin Yang.)*

The authors are with the College of Mechatronics Engineering and Automation, National University of Defense Technology, Changsha 410073, China (e-mail: yangxin.cambridge@foxmail.com; linzhikai0214@foxmail.com; 947152770@qq.com; lzq@maglev.cn).

Color versions of one or more of the figures in this paper are available online at http://ieeexplore.ieee.org.

Digital Object Identifier 10.1109/TPEL.2018.2812732

See http://www.ieee.org/publications_standards/publications/rights/index.html for more information.

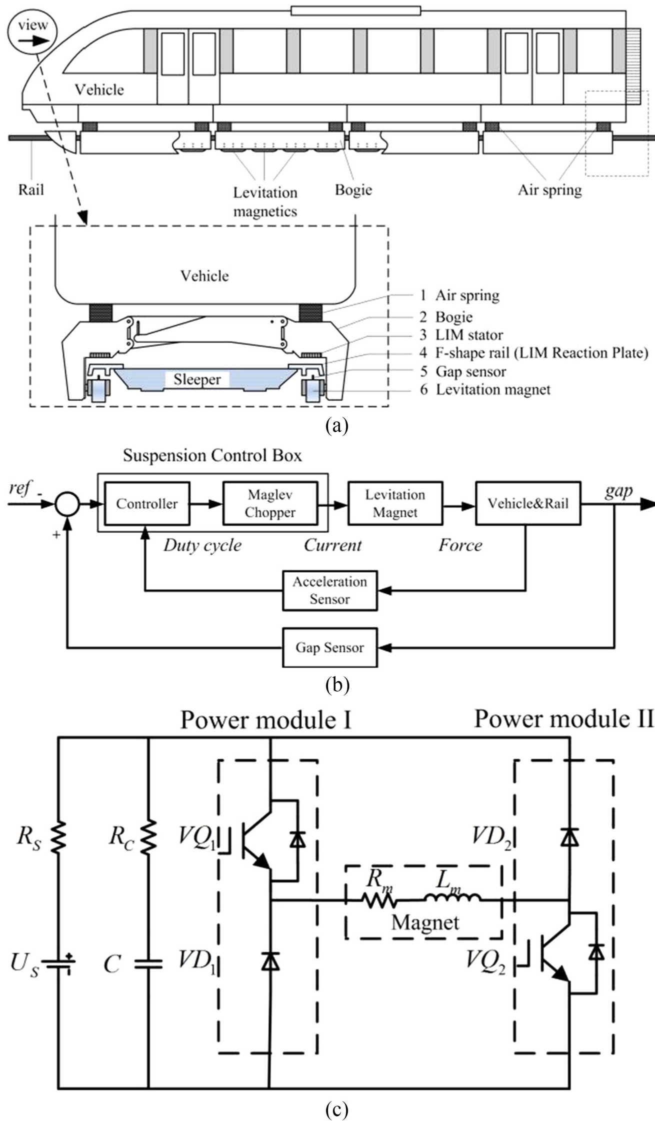

Fig. 1. (a) Principle of medium/low-speed maglev train. (b) Suspension control principle diagram. (c) Suspension chopper circuit.

databases of power cycling tests collected over years for different manufacturers [13]. Those empirical models are the most widely used method for lifetime prediction of IGBT modules. Most of those models take into account of thermal stresses and assume the long-term damage accumulation to be linear. In the application of power electronic devices, lifetime is closely related to thermal stresses. Excessive thermal cycles would trigger a thermo-mechanical stress in the chip or package, eventually leading to fatigue or even failures. Thermo-mechanical fatigue would trigger several severe failure modes of IGBT modules, including solder creep, bond wire lift-off/heel cracking, metallization reconstruction, and so on [7]–[13]. In recent years, advanced wire bonding techniques have been applied suggesting that the bond wire lift-off failure mode might be avoided with certainty so more effort is being made to analyze solder layers in more detail [14]. More importantly, according to [7] and [15]–[17] the temperature cycle with heating time (the period where power losses are generated in the IGBT resulting in a temperature swing) below 1 min has a significant effect on the fatigue of bond wires, while much longer heating time will be more likely to induce the solder fatigue. As the power cycling of IGBT modules within suspension choppers has a comparatively large duration for temperature swings, solder fatigue is assumed to be the main mechanism for failure as in [18] and [19]. Classic empirical models describe the dependence of N_f (the number of cycles to failure) on temperature. The well-known Coffin–Mason model is modified by the Arrhenius approach [10] as

$$N_f = A \cdot \Delta T_j^{\alpha} \cdot \exp\left(\frac{Q}{R \cdot T_m}\right). \tag{1}$$

However, (1) was reported and recognized for inadequate projection of the thermal fatigue for solder interconnection. Solders begin to exhibit creep behavior at room temperature (already greater than half the absolute melting temperature) [20]. A reasonable fatigue model must account for the effects of relaxation phenomena [20]–[22]. An improved analytical model could be proposed as

$$N_f = A \cdot f^{n_1} \cdot \Delta T_j^{\alpha} \cdot \exp\left(\frac{Q}{R \cdot T_m}\right) \tag{2}$$

where R is the gas constant 8.314 J/mol·K, T_m is the mean temperature in Kelvin, f is the power cycling frequency, and n_1 is the power of f. $A = 640$, $\alpha = -5$, and $Q = 7.8 \cdot 10^4$ J·mol^{-1} (or 0.8 eV), which are obtained by accelerated power cycling tests for a specific packaging that is similar to the IGBT module packaging used in this paper [12]. Equation (2) introduces the pronounced effect of power cycling frequency. The correction factor n_1 can account for creep rupture when $n_1 = 1$, in which failure only depends on time.

However, the problem lies in the fact that both the historical data in handbooks and from accelerated lifetime tests may be intended for a different application from the one studied [23], [24]. Also, both methods cannot provide a deeper physical description of the observed wear-out failure mechanism. Therefore, several physics-of-failure lifetime models are proposed [23]–[27]. Extracting temperature curves under their corresponding mission profiles, physical lifetime models are more attractive for assessment of power devices' lifetimes. To develop an accurate lifetime model of solder joint wear-outs, an energy-based method is first introduced in [25], which only took into account time-dependent creep of solder joints. Kovacevic *et al.* [14], [21], and [22] further consider elastic and plastic deformation of solder joints. Material parameters can be found in the literature and geometry-related parameters can be calculated using finite element simulation [27]. In this paper, two daily mission profiles of suspension choppers are considered and compared using the energy-based approach proposed in [21] and [22]. From our analysis, the mission profile where the maglev train operates without landing during operation hours is expected to survive much longer.

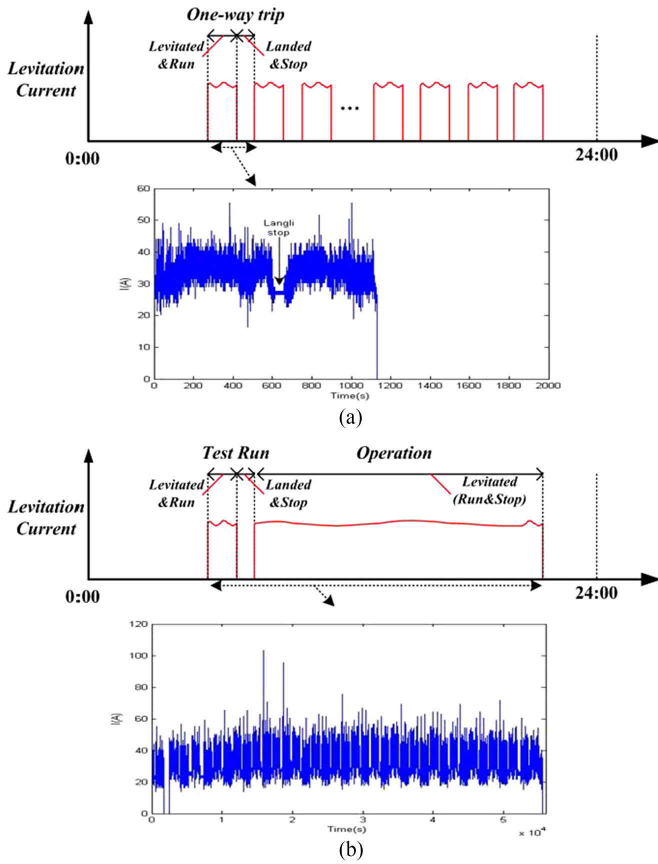

Fig. 2. (a) Levitation current of a single one-way trip in mission profile I. (b) Levitation current of mission profile II during a working day.

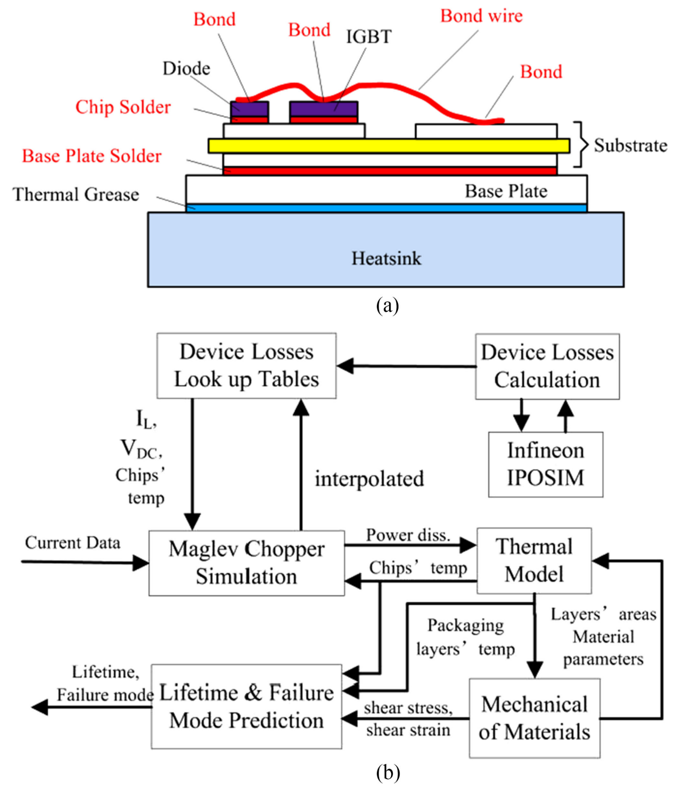

Fig. 3. (a) Construction of a standard IGBT module [17]. (b) Block diagram of lifetime prediction simulation.

II. Mission Profiles of Suspension Choppers

Each carriage of CME maglev trains contains five bogies. Each bogie is made of two suspension magnetic modules located on both sides of the track. Each magnet module contains four coils, every two of which are controlled by one suspension control box. A suspension control box is composed of suspension control DSPs, sensors, and suspension choppers [1]. A maglev carriage is supported by ten suspension control boxes. Due to the usage of a mechanical bogie, the mutual mechanical interaction between magnetic modules under a carriage is decoupled. Each suspension control box operates individually. All the suspension control boxes share a similar operation condition. The main circuit of one suspension chopper is shown in Fig. 1(c). The power part is constituted by two Infineon FF300R12KT3 IGBT modules. The suspension chopper input voltage is 300 V dc, providing unidirectional current for the load electromagnet with a switching frequency of 5 kHz. Such a selection of over-rating IGBTs is a redundancy consideration for a larger engineering safety and reliability margin.

There are generally two mission profiles for CME suspension choppers, as shown in Fig. 2(a) and (b). The cycle of each mission profile is one day. For mission profile I, as shown in Fig. 2(a), the train is levitated at the start of each one-way trip when levitation current is initiated. The single one-way trip from Changsha International Airport Station to Changsha South Railway Station (or the reversed way) lasts about 20 min. It is landed at the end of this trip when the current drops to zero. Normally, the train waits for around 10 min before the next trip starts. A typical profile of the levitation current in a one-way trip cycle is plotted in Fig. 2(a). The levitation current for each suspension chopper will be composed of tens of "pulses" during a working day. Fig. 2(b) illustrates mission profile II. In this case, the train will carry out a test run at the every start of a working day. At the end of the test run, the train will be landed to wait for an operation instruction. After receiving the instruction, the train will be levitated afterward whenever the train is moving or stops. The train will be landed only at the end of the whole working day. As a result, the levitation currents will keep flowing until the end of the day. The small ripples on the dc levitation current are the effect of suspension control. The measured current data of one typical suspension chopper under these two mission profiles are both demonstrated. The current sensor is LA 205-S/SP1 from LEM, which is installed inside the suspension control system. The sample frequency is 10 Hz. As it has been pointed out, the solder fatigue is assumed to be the main failure mechanism in our study; each power cycle lasts about tens of minutes. Thus, such a low sampling frequency will be enough to present junction temperature curves under both mission profiles.

III. Lifetime Prediction Framework of IGBT Modules

The construction of a standard IGBT module is shown in Fig. 3(a) [17]. It is composed of multiple layers made out of

different materials, such as silicon, solder, ceramic, copper, etc. The failure mechanisms that are most frequently observed in IGBTs mainly result from thermo-mechanical fatigue stresses experienced by those packaging materials. The main driving forces of such failure mechanisms are the mismatch in the coefficient of thermal expansion of different materials in the chip/package under temperature swings.

Therefore, lifetime prediction of IGBT modules normally requires an accurate temperature curve under a typical mission profile. A temperature-sensitive electrical parameter method is usually adopted to detect the virtual junction temperature that indicates the average temperature of an IGBT [28]. However, the junction temperature of IGBTs and diodes in current suspension choppers is unable to be measured online. The measurement devices of the junction temperature are unavailable in our current design. Therefore, an electro-thermal *RC* model is utilized for offline analysis. Parameterization of the thermal network could be realized from the heating curves of IGBT junction and case temperature measured on a power cycling [29]. A lifetime prediction simulation framework considering the detailed device physics as well as a comprehensive thermal model has been proposed in [30] for reduction in computational cost. Using look-up tables of devices' power losses as a function of load currents and their operating temperatures offers an improved compromise between computation speed and accuracy.

The proposed overall framework of IGBT modules' lifetime prediction simulation is shown in Fig. 3(b). It consists of several stages. Device losses are obtained using the online simulation tool IPOSIM of Infineon [31]. The loss look-up tables of IGBT/diode are shown in Fig. 4. The tables contain both switching and conduction losses. The gate resistor is 10 Ω to mitigate the switching ringing. The levitation current data from a mission profile are used for simulation. Initially, it finds out the corresponding power dissipation at the initial temperature. The obtained instantaneous power dissipation could be used to calculate the instantaneous junction temperature through the thermal *RC* network. The obtained junction temperature joining in the newly inputted current data determines the updated power dissipation at the new operation condition. As a result, the closed-loop simulation is formed. The junction temperature curves under different mission profiles can be estimated. Finally, lifetime models are used to analyze the obtained junction temperature curves.

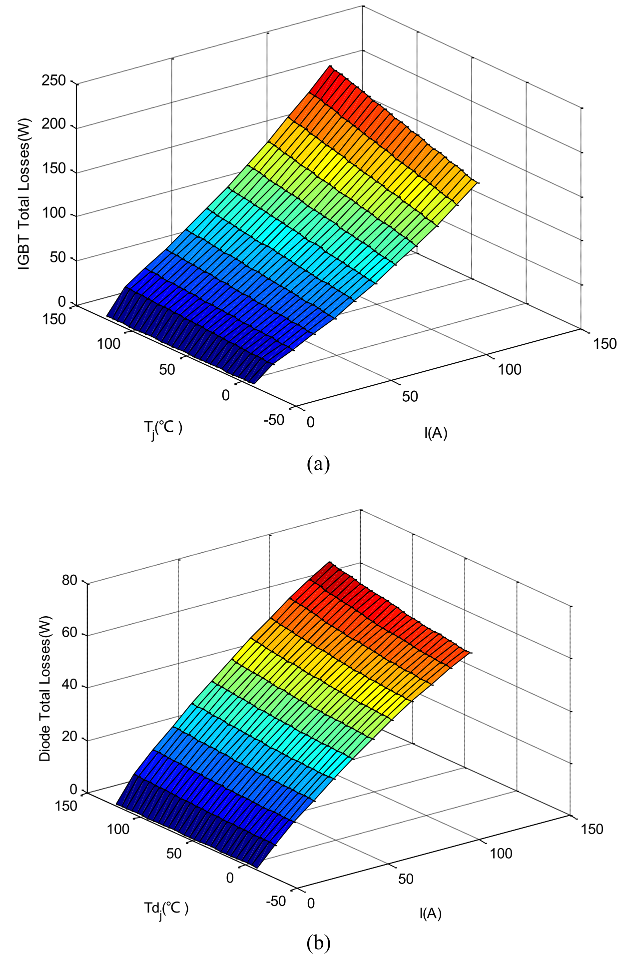

Fig. 4. (a) IGBT losses look-up table. (b) Diode losses look-up table

A. IGBT Module Thermal Model

A one-dimensional (1-D) thermal model is applied to simulate the temperatures of IGBT/diode chips, as shown in Fig. 5(a). As there is only one active IGBT in each module of the suspension chopper, the thermal coupling between active IGBTs and its paralleled freewheeling diodes is negligible [32]. Due to the distance between active chips, i.e., IGBTs and freewheeling diodes (not the parallel diode of IGBT), the thermal model of IGBTs and freewheeling diodes is calculated independently here. The active devices are the IGBTs (VQ1 and VQ2) and freewheeling diodes (VD1 and VD2), as shown in Fig. 1(c). The thermal impedance junction-to-heat sink of the IGBT module is modeled as a multilayer Foster *RC* network, and the heat sink is modeled as a second-order *RC* thermal network [33].

In Fig. 5(a), P_{tot} is power dissipation; $R11$ to $R14$ are thermal resistances, and $C11$ to $C14$ are thermal capacitances of IGBT; similarly, $R21$ to $R24$ are thermal resistances and $C21$ to $C24$ are thermal capacitances of freewheeling diode; R_{ich} and R_{dch} are the case to heat sink thermal resistances of IGBT and diode, respectively, and R_{ha} and C_{ha} are the thermal resistances and thermal capacitances of heat sink to ambient. The model parameters from junction-to-heat sink can be obtained by the datasheet from the IGBT module manufacturer [34]. The electro-thermal model is implemented in MATLAB/simulation, as shown in Fig. 5(b).

B. Thermal Impedance Extraction of the Heat Sink

The thermal network parameters of the heat sink can be extracted by using the simulated curve of case temperature to fit the experimentally measured curve. An experiment test rig is designed in Fig. 6(a). The proposed thermal measurement system includes thermocouples (type K from OMEGA), temperature transmitters (ws90501 from Huadian Automation), and a data acquisition card (NI USB-6008). Four measurement points (T1–T4) underneath the center of IGBT/diode chips are labeled. An

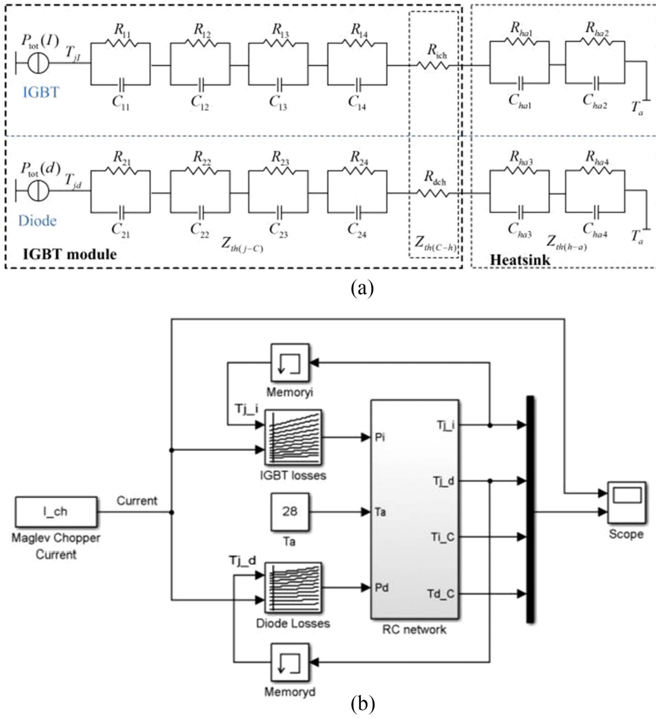

Fig. 5. (a) Thermal network of suspension chopper. (b) Electro-thermal model implemented in MATLAB/Simulink.

TABLE I
THERMAL NETWORK PARAMETERS OF THE HEAT SINK

Thermal resistance (K/W)	R_{ha1}	R_{ha2}	R_{ha3}	R_{ha4}
Value	0.22	0.255	0.19	0.58
Thermal capacitance (J/K)	C_{ha1}	C_{ha2}	C_{ha3}	C_{ha4}
Value	50	950	100	600

open-loop control is adopted where the duty cycle is set to providing a constant levitate current of 35 A. Four notched lines are made on the surface heat sink for the installation of thermocouples. The thermocouples are attached underneath the chips, as shown in Fig. 6(b). The silicon grease is evenly distributed. The diameter of the used thermocouples is comparatively small so its influence on the thermal impedance is ignored. T2 point measures diode VD2 and T4 point measures IGBT VQ2.

T1 and T3 measure the inactive chips. T1 and T3 have very small temperature swings so their curves are shown here. Only the T2 and T4 results are shown in Fig. 6(c). The thermal impedance of the heat sink is extracted by making the simulated case temperature curve to approach the measured curve. The optimal thermal parameters of the heat sink could be obtained, as shown in Table I. Fig. 6(c) shows that the simulated curve will fit the experimental data.

IV. Energy-Based Lifetime Model

An energy-based physical lifetime model is proposed to take the deformation mechanisms of IGBTs invoked under complex power cycles into account [14], [21], [22]. This model is based on the assumption that the solder joints are the weakest

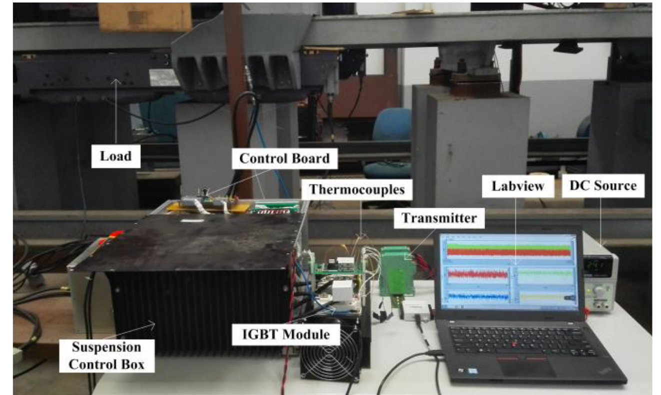

(a)

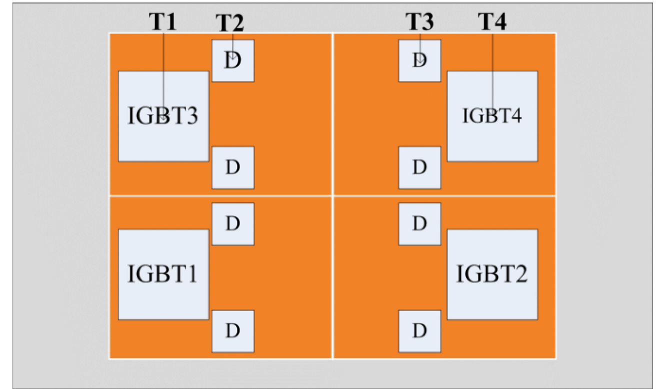

(b)

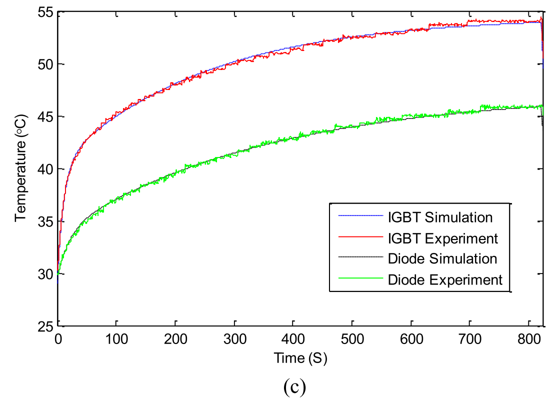

(c)

Fig. 6. (a) Experimental test rig setup. (b) Measured points underneath the power devices. (c) Simulated and measured case temperature curves, IGBT (VQ2) and diode (VD2).

points inside power module. The solder response to a thermal cycling load can be described by means of a hysteresis loop. The stress–strain response is modeled by solder constitutive equations that mathematically describe time-independent elastic and plastic deformations and time-dependent creep. Elastic behavior is described by Hooke's law according to which elastic shear strain γ_{el} can be expressed as the ratio between stress τ and temperature-dependent material shear modulus as follows:

$$\gamma_{\mathrm{el}} = \frac{\tau}{G\,(T)}. \tag{3}$$

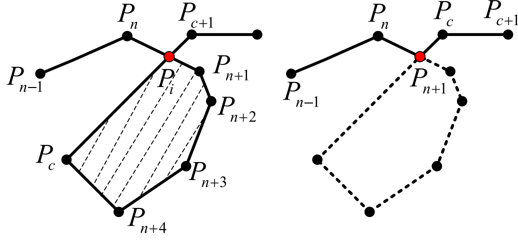

Fig. 7. Example of calculating a hysteresis loop area [38].

The temperature dependence of shear modulus is typically expressed by

$$G(T) = G_0 - G_1(T - 273) \tag{4}$$

where G_0 is the shear modulus at 0 °C and G_1 the temperature correction factor.

To describe time-independent plastic behavior Darveaux's stress–strain dependence is used as follows:

$$\gamma_{\mathrm{pl}} = C_p \left(\frac{\tau}{G(T)}\right)^{m_p} \tag{5}$$

where C_p is the plastic strain coefficient, and m_p is the sensitivity of plastic strain.

Analyzing the creep nature of 63Sn37Pb solder, two types of creep deformation can be distinguished: dislocation-controlled creep at higher and diffusion-controlled creep at lower stress levels, defined, respectively, by

$$\frac{d\gamma}{dt} = C_l \cdot \frac{G(T)}{T}\left[\sinh\left(\frac{\alpha\cdot\tau}{G(T)}\right)\right]^{n_l} \cdot e^{-Q_l/RT} + C_h \cdot \frac{G(T)}{T}\left[\sinh\left(\frac{\alpha\cdot\tau}{G(T)}\right)\right]^{n_h} \cdot e^{-Q_h/RT} \tag{6}$$

$$\frac{d\gamma}{dt} = B_1 \frac{G(T)}{T}\cdot\left(\frac{\tau}{G}\right)\cdot e^{-Q_b/RT} + B_2 \frac{G(T)}{T}\cdot\left(\frac{\tau}{G}\right)\cdot e^{-Q_m/RT}. \tag{7}$$

The constants and parameters for 63Sn37Pb solder can be found in [35] and [36]. With the input of junction temperature profiles, the stress–strain response of a solder joint can be generated by means of Clech's algorithm [37]. When the accumulated deformation energy reaches the critical value W_{tot}, it indicates that the device fails. W_{tot} is believed to be a constant for a given module design [14].

Due to the discrepancy of the sampling point, the closed hysteresis enclosed by the stress–strain curve itself will be an arbitrary shape of the polygon. The deformation energy of a mission profile could be calculated, as demonstrated in Fig. 7. The following algorithm is used to calculate the deformation energy of a mission profile.

Mark l_c as the current line segment and l_n as the line segment that intersects with l_c (not containing two lines overlap). P_i is the intersection of the two lines. The calculation process is [38]

1) Read next point P_{c+1}; P_c and P_{c+1} constitutes a line segment l_c. If this is the last point, go to step (5).
2) Determine whether the current line segment l_c intersects with previous line $l_{c-2}, l_{c-3}, \ldots l_1$. If l_c does not intersect with other lines, then mark the point P_{c+1} as P_c and returned to step (1); else, the intersection point P_i is calculated.
3) According to the two line segments (l_c, l_n) and intersection point P_i, all the vertices $P_i, P_{n+1}, \ldots P_c$ of the closed polygon can be obtained. The polygon area for the hysteresis energy accumulation can be calculated.
4) Remove all the vertices of the closed polygon expect the intersection P_i; change P_i to P_{n+1}, mark the point P_{c+1} as P_c, and return to step (1).
5) Output the energy value and the algorithm is finished.

V. Results

Before carrying out lifetime evaluation, finite element simulation is adopted to check the estimation of the junction temperature of IGBTs. Tables II and III present the related design parameters of the IGBT module used in this paper, which are generalized from [39]–[44]. Fig. 8(a) shows that at the steady situation the junction temperatures at T2 and T4 are very close to those from the *RC* thermal model. The 1-D *RC* model used in this paper is proven to be able to produce an average junction temperature with a satisfactory degree of accuracy. Using the simulation model described in Section II, the real-time junction temperature curves of IGBT and diode under the two different mission profiles are shown in Fig. 8(b) and (c), respectively. The ambient temperature here is considered to be under the worst condition. The surface temperature of the rail in Changsha is measured to be around 55 °C maximally in summer.

Then, the energy-based lifetime model presented in the previous section is used. W_{tot} needs to be calculated in advance. The power cycling data from accelerated aging experiments are used [12] where the IGBT junction temperature curves under those power cyclings are simplified by sawtooth waves to calculate the deformation energy of a single power cycle.

N_f can be calculated by the following equation:

$$N_f = W_{\mathrm{tot}} \cdot \Delta W^{-m} \tag{8}$$

where *m* depends on the solder type, and in case of tin–lead solder it is often reported to be $m \approx 1$ [21], and ΔW is the deformation energy loss caused by a single thermal cycle. The data, whose experimental conditions are closest to that as shown in Fig. 8, are selected. The medium temperature of the power cycling is 80 °C. The device ON-time t_{on} and OFF-time t_{off} of the power cycling are both maximally set as 3.14 s. The temperature swing varies from 30 to 80 °C. As shown in Fig. 9(a), the stress–strain curves for a single thermal cycle under different temperature swings are plotted using Cleth's algorithm [37]. ΔW under different temperature swings can be calculated. The total deformation energy W_{tot} is assumed to constant whatever the temperature swing varies [14]. According to (8), a linear curve must be fitted between N_f and ΔW^{-m}. So the total deformation energy W_{tot} and the parameter *m* in (8) can be calculated to be 2.5973×10^6 and 1.154 using the six chosen

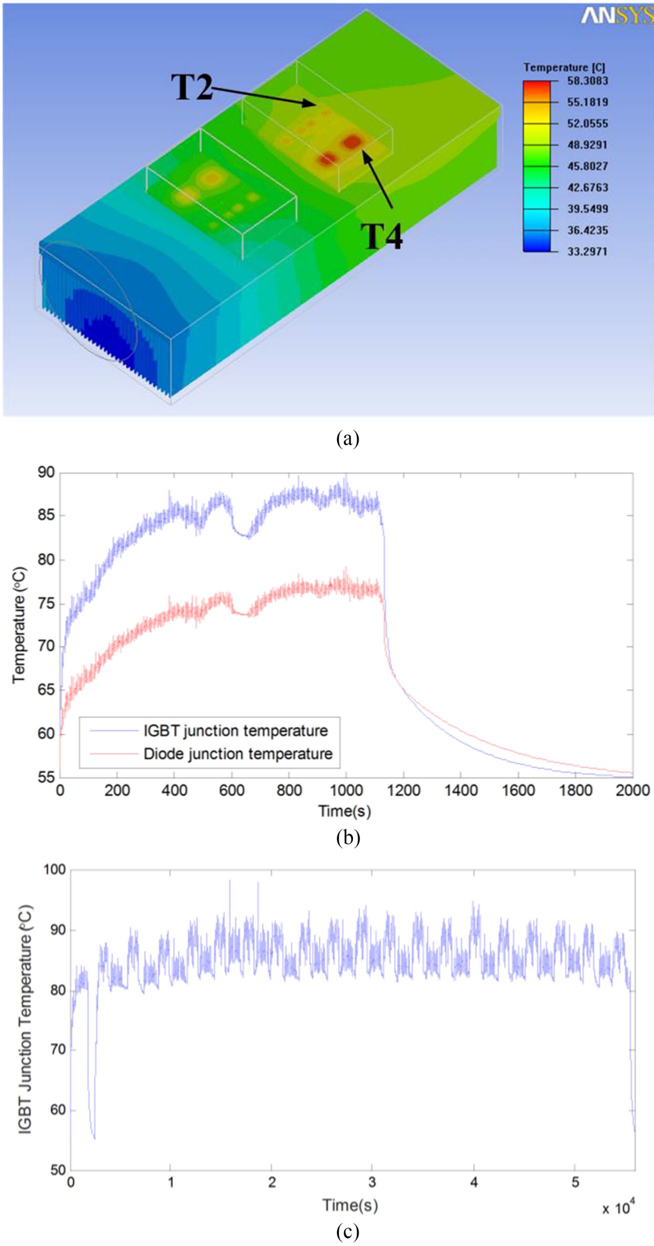

Fig. 8. (a) 3-D FEM result of a suspension chopper. (b) Simulated junction temperature of mission profile I (one way). (c) Simulated junction temperature of mission profile II.

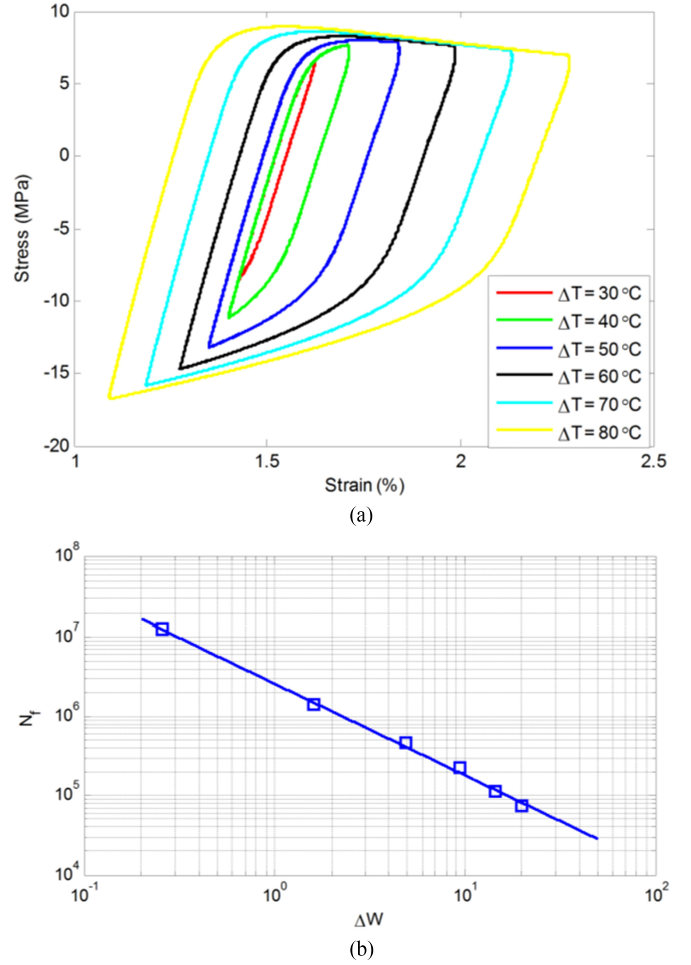

Fig 9. (a) Stress–strain response to different temperature swings. (b) Number of cycles to failure N_f as a function of ΔW.

sets of ΔW. The plot of N_f with variance of ΔW under different temperature swings is shown in Fig. 9(b).

For the two mission profiles, the stress–strain curves for IGBT modules can be seen in Fig. 10. The simulated accumulated deformation energy in each working day could be calculated. Fig. 10(a) shows the stress–strain plot using the current data in Fig. 2(a). This is the result of only a one-way trip. The accumulated deformation energy under this mission profile in a working day is 11.5062 (the area of the loop) in Fig. 10(a) multiplying 38 (the number of one-way trips in a working day). Fig. 10(b) shows the result of mission profile II in a whole day. The accumulated deformation energy of the loop in Fig. 10(b) is 143.7892. As the temperature swing is very small, the accumulation of deformation energy is regarded as linear [45]. The lifetime for mission profile I L_1 is found to be 11.17 years, while the lifetime for mission profile II L_2 is found to be 23.03 years as follows:

$$L_1 = \frac{2.5973 \times 10^6}{365 \times 38 \times (11.5062)^{1.154}} = 11.17 \quad (9)$$

$$L_2 = \frac{2.5973 \times 10^6}{365 \times (143.7892)^{1.154}} = 23.03. \quad (10)$$

VI. Discussion

The reliability of suspension choppers is of crucial importance for the development of maglev trains. The mission profile of IGBT modules in suspension choppers is different from that in the applications of electric vehicles or renewable energy. Although the load current swing of suspension choppers under both mission profiles is much less than that in electric vehicles or power converters of the wind plant, the reliability requirement of suspension choppers is much higher. The suspension choppers responsible for stable and safe suspension of maglev train tolerate no failure or wear-out at operation. As heated efforts are

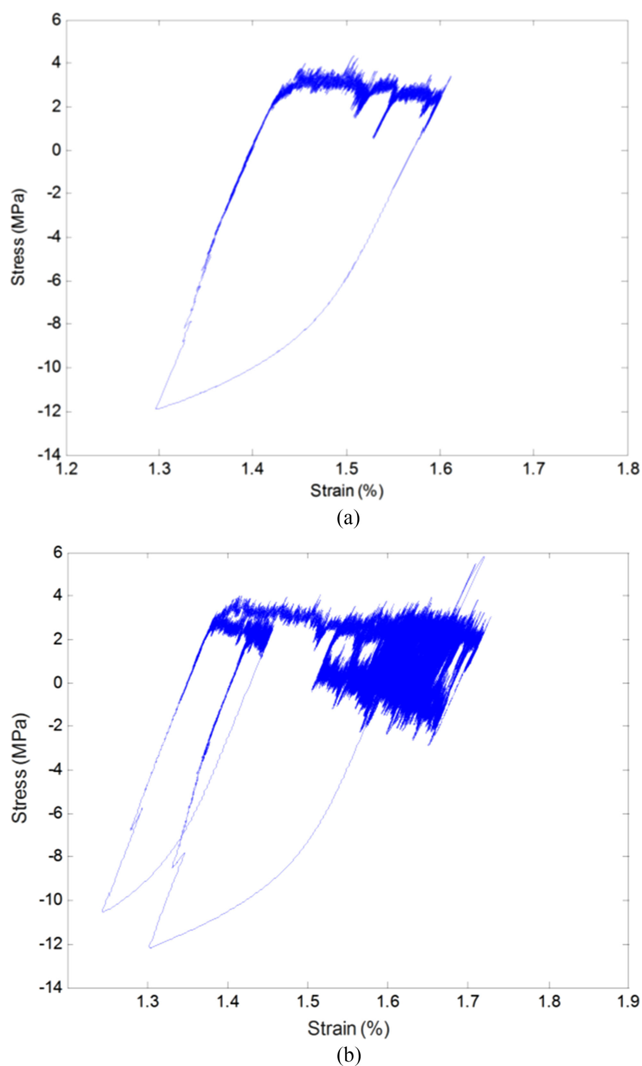

Fig. 10. (a) Stress–strain curve for a single one-way trip for mission profile I. (b) Stress–strain curve for mission profile II.

made to further increase the speed of the current medium/low-speed maglev trains, the safety and reliability requirement will be even harsher. Therefore, the investigation into the reliability of suspension choppers is of great necessity.

Furthermore, both mission profiles show very interesting load patterns. For mission profile I, it resembles the widely used accelerated aging tests except that its duration of such a temperature swing is smaller. For mission profile II, IGBT modules work in a very large working cycle based on days, which has been rarely analyzed in previous publications. The thermal stress is also comparatively small. The time-dependent creep of soldering might be the dominant factor in influencing its lifetime instead of frequency harsh temperature swings. Unlike the randomness in other heated research background, the operation condition of suspension choppers is very predictable. In this paper, an energy-based physical method is used for lifetime prediction of the key component IGBT in suspension choppers at the worst environmental conditions. This could provide an important reference for maintenance of suspension choppers. Different lifetime values are obtained. Mission profile II seems to have much longer lifetimes, more than double that of mission profile I, which could be easily interpreted by much reduced temperature variance. However, it is at the expense of much increased suspension power losses as the current would remain even when the train stops (currently, the suspension power is approximately 1 kW/ton at moving, 0.8 kW/ton at stop if the train is still levitated). For both mission profiles, that means the total levitation energy consumption will be increased over 30%, giving an approximate increased energy consumption of 90 kWh for a carriage (about 28 tons at no load) per day. If the full load operation is considered, the number could be even larger. A tradeoff between IGBT lifetime and levitation energy consumption has to be made here.

Future work might be needed to design reliable experiment tests on IGBT modules to further investigate the fatigue and failure mechanism under these operation conditions and optimize the physical lifetime model used in this paper. Also, the tradeoff between lifetime (related to maintenance cost) and suspension power losses is also needed for further investigation. The failure judgment criterion W_{tot} might further need optimization by assistance of finite element analysis of mechanical and thermal simulation [27]. Also, in this paper, the worst operation temperature is considered, more accurate prediction might be needed to consider the overall environmental temperature variance following advanced analysis methods that have been investigated in [7]–[9].

The accuracy of the junction temperature curve could be further improved. The estimation of power losses in this paper could be further improved. The online software IPOSIM does not consider the impacts of stray inductances in the circuits, which has been shown has great impacts on the power losses as well as stability [46], [47]. This would cause inaccuracies in the junction temperature estimation. Measured power losses data are needed. To further improve the accuracy of temperature estimation, the thermal model might need improvement by considering the thermal coupling between the active IGBT and freewheeling diode. In that way, the transient temperature profile could be more accurate enabling even better lifetime predictions.

VII. Conclusion

This paper analyzes the lifetimes of a typical suspension chopper under two typical daily mission profiles. An overall simulation framework of IGBT modules' lifetime prediction is provided. Using look-up tables of IGBT and diode losses, a widely used 1-D *RC* thermal network is established to simulate the device junction temperature profile. A test rig is built for the IGBT/diode case temperature measurement. The thermal impedance parameterization of the heat sink is achieved nicely by optimizing fitting between the simulated case temperature curve and the experimentally measured temperature curve. A satisfactory fitting is obtained. Therefore, the junction temperature profiles under two considered mission profiles are estimated. By using an energy-based physical lifetime model, time-independent elastic and plastic deformations and

time-dependent creep are mathematically described. This model is based on Clech's algorithm to simulate the stress–strain solder response under cyclical thermal loading. Such an energy-based lifetime modeling approach provides numerical simulation of lifetime results with a high degree of confidence as information within the mission profiles is well considered. The worst environmental temperature is used for a minimum lifetime evaluation, which can provide an important reference for suspension chopper maintenance. By comparison, the daily mission profile where maglev trains operate without landing during operation is concluded to have a much longer lifetime.

APPENDIX

TABLE II
THERMAL PROPERTIES OF MATERIALS OF IGBT MODULES

Layer	IGBT	Diode	Solder	Copper	Al_2O_3	Baseplate
Thickness (mm)	0.12	0.12	0.1	0.35	0.6	3

TABLE III
THERMAL PARAMETERS AND THICKNESS OF EACH LAYER IN IGBT MODULES

Layer	Coefficient δ_{ts} time-scaling	Thermal conductivity $(W{\cdot}m^{-1}{\cdot}K^{-1})$	Density $(kg{\cdot}m^3)$	Specific heat capacity $(J{\cdot}kg^{-1}{\cdot}K^{-1})$
IGBT	1	163	2330	703
Diode	1	163	2330	703
Al_2O_3	1	27	3900	900
Solder	1	50	9000	150
Copper	1	400	8700	385
Baseplate	1	400	8700	385

REFERENCES

[1] Z. Liu, Z. Long, and X. Li, *Maglev Trains Key Underlying Technologies (Springer Tracts in Mechanical Engineering)*. Berlin, Germany: Springer, 2015.

[2] L. Yan, "Development and application of the maglev transportation system," *IEEE Trans. Appl. Supercond.*, vol. 18, no. 2, pp. 92–99, Jun. 2008.

[3] H.-W. Lee, K.-C. Kim, and J. Lee, "Review of maglev train technologies," *IEEE Trans. Magn.*, vol. 42, no. 7, pp. 1917–1925, Jul. 2006.

[4] J. H. Jeong, C. W. Ha, J. Lim, and J. Y. Choi, "Analysis and control of electromagnetic coupling effect of levitation and guidance systems for semi-high-speed maglev train considering current direction," *IEEE Trans. Magn.*, vol. 53, no. 6, Jun. 2017, Art. no. 8300204.

[5] H. Oh, B. Han, P. McCluskey, C. Han, and B. D. Youn, "Physics-of-failure, condition monitoring, and prognostics of insulated gate bipolar transistor modules: A review," *IEEE Trans. Power Electron.*, vol. 30, no. 5, pp. 2413–2426, May 2015.

[6] *Military Handbook: Reliability Prediction of Electronic Equipment*, Standard MIL-HDBK-217F, Dec. 1991.

[7] P. D. Reigosa, H. Wang, Y. Yang, and F. Blaabjerg, "Prediction of bond wire fatigue of IGBTs in a PV inverter under a long-term operation," *IEEE Trans. Power Electron.*, vol. 31, no. 10, pp. 7171–7182, Oct. 2016.

[8] U. M. Choi, F. Blaabjerg, and S. Jørgensen, "Study on effect of junction temperature swing duration on lifetime of transfer molded power IGBT modules," *IEEE Trans. Power Electron.*, vol. 32, no. 8, pp. 6434–6443, Aug. 2017.

[9] U. M. Choi, K. Ma, and F. Blaabjerg, "Validation of lifetime prediction of IGBT modules based on linear damage accumulation by means of superimposed power cycling tests," *IEEE Trans. Ind. Electron.*, vol. 65, no. 4, pp. 3520–3529, Apr. 2018.

[10] D. Hirschmann, D. Tissen, S. Schröder, and R. W. De Doncker, "Reliability prediction for inverters in hybrid electrical vehicles," in *Proc. 37th IEEE Power Electron. Spec. Conf.*, Jeju, South Korea, 2006, pp. 1–6.

[11] D. Astigarrage *et al.*, "Analysis of the results of accelerated aging tests in insulated gate bipolar transistors," *IEEE Trans. Power Electron.*, vol. 31, no. 11, pp. 7953–7961, Nov. 2016.

[12] M. Held, P. Jacob, G. Nicoletti, P. Scacco, and M. H. Poech, "Fast power cycling test of IGBT modules in traction application," in *Proc. 2nd Int. Conf. Power Electron. Drive Syst.*, 1997, pp. 425–430.

[13] ABB Application Note, "Load-cycling capability of HiPakTM IGBT modules," 2012

[14] I. F. Kovacevic, U. Drofenik, and J. W. Kolar, "New physical model for lifetime estimation of power modules," in *Proc. Int. Power Electron. Conf.*, Sapporo, Japan, 2010, pp. 2106–2114.

[15] L. Yang, P. A. Agyakwa, and C. M. Johnson, "Physics-of-failure lifetime prediction models for wire bond interconnects in power electronic modules," *IEEE Trans. Device Mater. Reliab.*, vol. 13, no. 1, pp. 9–17, Mar. 2013.

[16] K. Ma, M. Liserre, F. Blaabjerg, and T. Kerekes, "Thermal loading and lifetime estimation for power device considering mission profiles in wind power converter," *IEEE Trans. Power Electron.*, vol. 30, no. 2, pp. 590–602, Feb. 2015.

[17] H. Wang, K. Ma, and F. Blaabjerg, "Design for reliability of power electronic systems," in *Proc. 38th Annu. Conf. IEEE Ind. Electron. Soc.*, Montreal, QC, Canada, 2012, pp. 33–44.

[18] D. Xiang, L. Ran, P. Tavner, A. Bryant, S. Yang, and P. Mawby, "Monitoring solder fatigue in a power module using case-above-ambient temperature rise," *IEEE Trans. Ind. Appl.*, vol. 47, no. 6, pp. 2578–2591, Nov./Dec. 2011.

[19] S. Yang, D. Xiang, A. Bryant, P. Mawby, L. Ran, and P. Tavner, "Condition monitoring for device reliability in power electronic converters: A review," *IEEE Trans. Power Electron.*, vol. 25, no. 11, pp. 2734–2752, Nov. 2010.

[20] K. C. Norris and A. H. Landzberg, "Reliability of controlled collapse interconnections," *IBM J. Res. Develop.*, vol. 13, no. 3, pp. 266–271, May 1969.

[21] G. J. Riedel, R. Schmidt, C. Liu, H. Beyer, and I. Alaperae, "Reliability of large area solder joints within IGBT modules: Numerical modeling and experimental results," in *Proc. 7th Int. Conf. Integr. Power Electron. Syst.*, Nuremberg, Germany, 2012, pp. 1–6.

[22] I. F. Kovacevic-Badstuebner, J. W. Kolar, and U. Shilling, "Modelling for the lifetime prediction of power semiconductor modules," in *Reliability of Power Electronic Converter System*. London, U.K.: IET, 2016, pp. 103–140.

[23] Y. Lu and A. Christou, "Lifetime estimation of insulated gate bipolar transistor modules using two-step Bayesian estimation," *IEEE Trans. Device Mater. Reliab.*, vol. 17, no. 2, pp. 414–421, Jun. 2017.

[24] K. B. Pedersen and K. Pedersen, "Dynamic modeling method of electro-thermo-mechanical degradation in IGBT modules," *IEEE Trans. Power Electron.*, vol. 31, no. 2, pp. 975–986, Feb. 2016.

[25] M. Ciappa, F. Carbognani, and W. Fichtner, "Lifetime prediction and design of reliability tests for high-power devices in automotive applications," *IEEE Trans. Device Mater. Reliab.*, vol. 3, no. 4, pp. 191–196, Dec. 2003.

[26] G. J. Riedel, R. Schmidt, C. Liu, H. Beyer, and I. Alaperae, "Reliability of large area solder joints within IGBT modules: Numerical modeling and experimental results," in *Proc. 7th Int. Conf. Integr. Power Electron. Syst.*, 2012, pp. 1–6.

[27] H. Lu and C. Bailey, "Reliability prediction for IGBT solder joints using Clech algorithm," in *Proc. 17th Int. Conf. Electron. Packag. Technol.*, 2016, pp. 1059–1063.

[28] B. Ji, V. Pickert, W. Cao, and B. Zahawi, "In situ diagnostics and prognostics of wire bonding faults in IGBT modules for electric vehicle drives," *IEEE Trans. Power Electron.*, vol. 28, no. 12, pp. 5568–5577, Dec. 2013.

[29] H. Huang and P. A. Mawby, "A lifetime estimation technique for voltage source inverters," *IEEE Trans. Power Electron.*, vol. 28, no. 8, pp. 4113–4119, Aug. 2013.

[30] A. T. Bryant, P. Mawby, P. Palmer, E. Santi, and J. Hudgins,"Exploration of power device reliability using compact device models and fast electro-thermal simulation," *IEEE Trans. Ind. Appl.*, vol. 44, no. 3, pp. 894–903, May 2008.

[31] "IPOSIM: IGBT power simulation tool." [Online]. Available: https://infineon.transim.com/iposim/Pages/inputs.aspx

[32] A. S. Bahman, K. Ma, P. Ghimire, F. Iannuzzo, and F. Blaabjerg, "A 3-D-lumped thermal network model for long-term load profiles analysis in high-power IGBT modules," *IEEE J. Emerging Sel. Topics Power Electron.*, vol. 4, no. 3, pp. 1050–1063, Sep. 2016.

[33] B. Waleri *et al.*, "Time resolved in situ Tvj measurements of 6.5 kV IGBT during inverter operation," in *Proc. Power Convers. Intell. Motion*, 2009, pp. 1–6.
[34] "IGBT module up to 1200 V – FF300R12KT3," Infineon. [Online]. Available: http://www.infineon.com
[35] H. L. J. Pang, Z. P. Wang, Q. J. Yang, and X. Q. Shi, "Creep behavior and deformation mechanism map of Sn-Pb eutectic solder alloy," *J. Eng. Mater. Technol.*, vol. 125, no. 1, pp. 81–88, 2003.
[36] G. Z. Wang, Z. N. Cheng, K. Becker, and J. Wilde, "Applying Anand model to represent the viscoplastic deformation behavior of solder alloys," *J. Electron. Packag.*, vol. 123, no. 3, pp. 247–253, 2001.
[37] J.-P. Clech, "Review and analysis of lead-free solder material properties." [Online]. Available: http://www.metallurgy.nist.gov/solder/clech/Introduction.htm
[38] Z. Lin *et al.*, "Lifetime prediction of power devices in maglev choppers using physics-based electro-thermo-mechanical model," in *Proc. Eur. Conf. Power Electron. Appl.*, 2017, pp. 1–7.
[39] X. Yang, M. Otsuki, and P. R. Palmer, "Physics-based insulated-gate bipolar transistor model with input capacitance correction," *IET Power Electron.*, vol. 8, no. 3, pp. 417–427, 2015.
[40] C. Batard, N. Ginot, and J. Antonios, "Lumped dynamic electrothermal model of IGBT module of inverters," *IEEE Trans. Compon., Packag. Manuf. Technol.*, vol. 5, no. 3, pp. 355–364, Mar. 2015.
[41] Y. Tang and H. Ma, "Dynamic electrothermal model of paralleled IGBT modules with unbalanced stray parameters," *IEEE Trans. Power Electron.*, vol. 32, no. 2, pp. 1385–1399, Feb. 2017.
[42] W. Lai *et al.*, "Experimental investigation on the effects of narrow junction temperature cycles on die-attach solder layer in an IGBT module," *IEEE Trans. Power Electron.*, vol. 32, no. 2, pp. 1431–1441, Feb. 2017.
[43] T. K. Gachovska, B. Tian, J. L. Hudgins, W. Qiao, and J. F. Donlon, "A real-time physical model for monitoring of power semiconductor devices," *IEEE Trans. Ind. Appl.*, vol. 51, no. 4, pp. 3361–3367, Jul./Aug. 2015.
[44] K. Ma, A. S. Bahman, S. Beczkowski, and F. Blaabjerg, "Complete loss and thermal model of power semiconductor including device rating information," *IEEE Trans. Power Electron.*, vol. 30, no. 5, pp. 2556–2569, May 2015.
[45] W. Lai, M. Chen, L. Ran, O. Alatise, S. Xu, and P. Mawby, "Low $\triangle$Tj stress cycle effect in IGBT power module die-attach lifetime modeling," *IEEE Trans. Power Electron.*, vol. 31, no. 9, pp. 6575–6584, Sep. 2016.
[46] X. Yang, Y. Yuan, Z. Long, J. Goncalves, and P. R. Palmer, "Robust stability analysis of active voltage control for high-power IGBT switching by Kharitonov's theorem," *IEEE Trans. Power Electron.*, vol. 31, no. 3, pp. 2584–2595, Mar. 2016.
[47] X. Yang, Z. Long, Y. Wen, H. Huang, and P. R. Palmer, "Investigation of the tradeoff between switching losses and EMI generation in Gaussian s-shaping for high-power IGBT switching transients by active voltage control," *IET Power Electron.*, vol. 9, no. 9, pp. 1979–1984, Jul. 2016.

Xin Yang (SM'12–M'15) received the B.Eng. degree in electrical engineering and its automation from the Huazhong University of Science and Technology, Wuhan, China, in 2009, the M.Sc. degree (with distinction) in analogue & digital IC design from Imperial College London, London, U.K., in 2010, and the Ph.D. degree in power electronics from the University of Cambridge, Cambridge, U.K., in 2014.

He is currently an Assistant Professor with the National University of Defense Technology, Changsha, China. His research interests mainly include power electronics, high-power semiconductor device modeling and simulation, and reliability of power converters.

Dr. Yang was the recipient of the Cambridge Overseas Scholarship, the Henry Lester Scholarship (three times), the IEEE Industrial Electronics Society Studentship (2013), and the Cambridge University Lundgren Fund. In 2017, he became one of the National Young Distinguished Experts (the Thousand Talents Plan, China). He is an Associate Editor for the *IET Power Electronics Journal*.

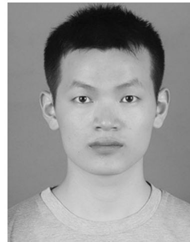

Zhikai Lin received the B.S. degree in measurement control technology and instruments from the Huazhong University of Science and Technology, Wuhan, China, in 2015, and the M.S. degree in electromagnetic levitation and propulsion technology from the National University of Defense Technology, Changsha, China, in 2018.

His research interests include power electronics and power electronic device reliability.

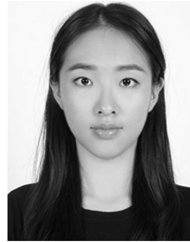

Jingfang Ding received the B.S. degree in automation from the Northeastern University, Shenyang, China, in 2016. She is currently working toward the Postgraduate degree at the National University of Defense Technology, Changsha, China.

Her research interests include magnetic levitation control, electromagnetic analysis, control theory, and control engineering.

Zhiqiang Long received the B.S. degree in automation from the Huazhong University of Science and Technology, Wuhan, China, in 1988, the M.S. degree in flight mechanics from the Harbin Institute of Technology, Harbin, China, in 1991, and the Ph.D. degree in control science and engineering from the National University of Defense Technology, Changsha, China, in 2010.

He is working with the National University of Defense Technology, as a Professor and currently is also the Head Research Engineer of the Engineering Research Center of Maglev Technology. His research interests include magnetic levitation control, fault diagnosis, tolerant control for maglev trains, and new maglev technology.